Stabilization of steady states in an array of all-to-all coupled oscillators

Arūnas Tamaševičius,* Skaidra Bumelienė, and Elena Adomaitienė
Center for Physical Sciences and Technology, 3 Saulėtekio ave., Vilnius LT-10257, Lithuania

(Received 13 January 2019; revised manuscript received 15 March 2019; published 30 April 2019)

An array of globally all-to-all coupled FitzHugh-Nagumo–type oscillators is considered. We suggest an adaptive first-order stable filter control feedback technique to stabilize the steady states of the oscillators. The overall system includes separate networks of coupling and control. Therefore, the controller does not depend on the intrinsic parameters of coupling between the oscillators. We have investigated stabilization of the steady states in an array of nonidentical oscillators analytically, numerically, and experimentally.

DOI: 10.1103/PhysRevE.99.042217

I. INTRODUCTION

A large number of various couplings between dynamical systems in general and, in particular, limit-cycle or chaotic oscillators have been introduced and considered in the literature (see, for example, Ref. [1] and references therein). Very recently, different networks of interacting units with distinct design principles have been reviewed [2]. From the point of view of network topology, there are three main classes of couplings. The first is *nearest-neighbors coupling* (also called local coupling), physically associated with the diffusive mechanism of interaction. Geometrically, it can be presented as a chain, ring, or lattice configuration. The second is *all-to-all* or *each-to-each coupling* (also called global coupling), physically characterized by the mean-field mechanism of interaction. The third is star coupling, where one distinguished central node (CN) is coupled to all oscillators [Fig. 1(a)]. Depending on the physical origin of the CN and the coupling mode, some specific cases of the star coupling can be attributed to global class of coupling. For example, if the CN is a common external driving unit (exciter), then star coupling represents a nonautonomous system with a common drive signal. This case is not considered as global coupling. However, if the CN is occupied by one distinguished oscillator (leader) of the array, then the situation depends on the mode of coupling (either *unidirectional* or *bidirectional*). In the case of unidirectional mode (from the CN toward the periphery), we come to the so-called master-slave(s) or drive-response configuration, that, again, is not global, whereas the case of a bidirectional mode ("weak leader") implicates the mean-field interaction, which is a characteristic feature of global coupling. Finally, if the CN is simply a common connecting node, bidirectionally coupled to the oscillators, then star coupling and all-to-all coupling coincide, since both of them are described by the mean-field mechanism of interaction between the oscillators. In a very special case, when the CN is "grounded" [3], the array becomes physically uncoupled. Thus, it no longer belongs to any class of coupling.

To summarize, there are two different global coupling configurations, namely bidirectional star coupling [Fig. 1(a)] and all-to-all coupling [Fig. 1(b)]. Obviously the term "global" applies to the case of $N \geqslant 3$ only. For $N = 2$ it is simply a bilateral coupling. We note that for $N = 3$ (as sketched in Fig. 1 for simplicity) all-to-all coupling formally coincides with nearest-neighbor coupling, specifically ring coupling, which, in general (for arbitrary N), is not global.

Any kind of coupling of oscillators (except for the star configuration with CN "grounded") eventually leads to synchronization—a universal phenomenon observed in a variety of natural systems and engineering [4]. In most cases, e.g., coupled spin-torque nano-oscillator arrays [5] and laser arrays [6], synchronization increases the output power. Thus, it has a favorable impact. However, sometimes it is an undesirable effect, for example, synchrony of neurons in the human brain. It is supposed that strong synchronization of neurons can cause the symptoms of Parkinson's disease [7,8]. A number of feedback techniques have been suggested to suppress synchrony of coupled oscillators. They employ, for example, repulsive coupling [3,9], mean-field nullifying [3,10], act-and-wait algorithm [11], time delay [7,12], a passive oscillator in the feedback loop [13], and a separate registration-stimulation setup [14].

The most straightforward way to get around the problem of undesirable synchrony is to suppress the activity of the oscillators. This can be achieved by externally driving the oscillators at high frequency (much higher than their natural frequencies) [15–17]. Another option to stabilize the intrinsic steady states of the oscillators by means of either the second-order damped oscillator (actually a band-pass filter) [13] or the first-order low-pass filter-based adaptive feedback technique [18].

The external high-frequency drive in neurology is known as deep brain stimulation (DBS), applying ≈100-Hz periodic pulses to certain brain areas [19]. DBS is a clinically approved therapy for patients with Parkinson's disease. Unfortunately, DBS often causes unpleasant side effects.

The above-mentioned feedback technique of stabilizing steady states [18] is limited to strong coupling of the oscillators. The coupling parameter k should exceed some threshold value. In many engineering systems the k can be easily adjusted to set a sufficient value. However, in natural systems,

*arunas.tamasevicius@ftmc.lt.

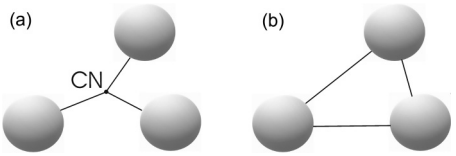

FIG. 1. Globally coupled oscillators. (a) Bidirectional star configuration; here CN is a simple connection node (not an oscillator); (b) all-to-all configuration.

e.g., in biological systems, k is an intrinsic parameter of the system, which is not easy to tune and, in general, its value is unknown. Therefore, it is important to develop a control technique independent of the intrinsic coupling strength.

In this paper, we consider all-to-all globally coupled oscillators with separate networks of coupling and control.

II. GLOBAL COUPLING

Let us consider an array of N globally coupled second-order limit-cycle oscillators:

$$\dot{x}_i = F(x_i, y_i) + Q(x_j, x_i), \tag{1}$$

$$\dot{y}_i = G(x_i, y_i), \quad i, j = 1, 2, \ldots, N. \tag{2}$$

Here $F(\ldots)$ is a nonlinear function, $G(\ldots)$ is either a nonlinear or linear function, and $Q(\ldots)$ is the coupling-control term.

For the star coupling configuration [Fig. 1(a)]:

$$Q(x_j, x_i) = Q(x_i) = k(X_{\mathrm{CN}} - x_i), \tag{3}$$

where k is the coupling coefficient and X_{CN} is the variable at the CN.

Control of the array is implemented by "manipulating" the variable at the coupling node, X_{CN}. There are four different cases for the variable X_{CN}.

(1) No control; presence of $\langle x\rangle$ leads to synchronization,

$$X_{\mathrm{CN}} = \frac{1}{N}\sum_{j=1}^{N} x_j = \langle x\rangle. \tag{4}$$

(2) "Grounding" the coupling node. The reason of synchronization is removed. Thus, it leads to desynchronization [3],

$$X_{\mathrm{CN}} = 0. \tag{5}$$

(3) Repulsive coupling [3,9]. This leads either to desynchronization or to synchronization at the same frequency but with the opposite phases distributed in the 2π phase circle. Both of them yield a low value of the mean-field variable $\langle x\rangle$,

$$X_{\mathrm{CN}} = -\langle x\rangle. \tag{6}$$

(4) Adaptive control via stable filter [18],

$$X_{\mathrm{CN}} = z; \quad \dot{z} = \omega_f(\langle x\rangle - z). \tag{7}$$

Here the auxiliary variable z is a filtered copy of $\langle x\rangle$ and $\omega_f \ll 1$ is the cut-off frequency of the filter.

For the all-to-all coupling configuration [Fig. 1(b)] the coupling term $Q(x_j, x_i) = Q(x_i)$ in the absence of control reads:

$$Q(x_i) = k\sum_{j=1}^{N}(x_j - x_i) = kN(\langle x\rangle - x_i). \tag{8}$$

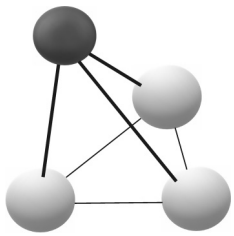

FIG. 2. Globally coupled all-to-all oscillators (light gray spheres) and a controller (dark gray sphere), coupled to all oscillators.

The structure of $Q(x_i)$ given by formula (8) is the same as in formula (3) with $X_{\mathrm{CN}} = \langle x\rangle$. However, its value is significantly different, since it is multiplied by a factor of N.

III. GLOBAL CONTROL

In the case of star coupling [Fig. 1(a)] the control is achieved via a single node, CN. Though the bidirectional star coupling is global, the control can be considered a quasilocal technique, whereas for all-to-all coupling [Fig. 1(b)] there is no specified central node. Moreover, in natural arrays, e.g., biological systems, the structure of the coupling configuration cannot be changed, and the coupling coefficient k cannot be adjusted. Therefore, the control should be implemented globally via applying the controller to all oscillators (Fig. 2). Consequently, we add to the coupling term $Q(x_j, x_i)$, given by formula (8), an independent control term $q(z - x_i)$:

$$Q(x_j, x_i) = kN(\langle x\rangle - x_i) + q(z - x_i),$$
$$\dot{z} = \omega_f(\langle x\rangle - z). \tag{9}$$

Here, in contrast to the coupling coefficient k, the value of control coefficient q can be set arbitrarily by an external controller.

Further, to be specific, we consider control of an array of all-to-all coupled FitzHugh-Nagumo (FHN)–type oscillators [18]:

$$\dot{x}_i = f(x_i) - y_i - c_i + kN(\langle x\rangle - x_i) + q(z - x_i), \tag{10}$$

$$\dot{y}_i = x_i - by_i, \quad i = 1, 2, \ldots, N, \tag{11}$$

$$\dot{z} = \omega_f(\langle x\rangle - z). \tag{12}$$

Here the $f(x_i)$ is a three-segment piecewise linear strongly asymmetric ($d \gg g \geqslant 0$) function,

$$f(x_i) = ax_i - \begin{cases} d(x_i + 1), & x_i < -1, \\ 0, & -1 \leqslant x_i \leqslant 1, \\ g(x_i - 1), & x_i > 1. \end{cases} \tag{13}$$

The mean-field variable $\langle x\rangle$ is defined as

$$\langle x\rangle = \frac{1}{N}\sum_{i=1}^{N} x_i. \tag{14}$$

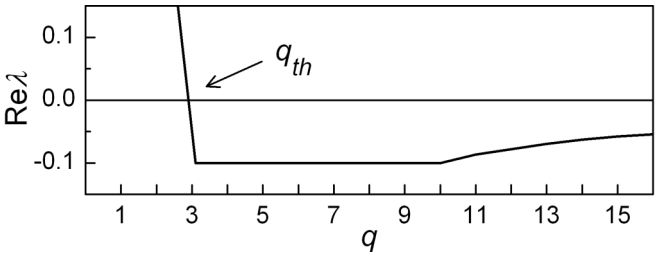

FIG. 3. Maximal value of the real parts of the eigenvalues $\lambda_{1,2,3}$, Reλ vs. the control parameter q. The arrow indicates the threshold parameter $q_{\rm th} = 2.9$. $a = 3$, $b = 0.1$, $\omega_f = 0.1$.

Equations (10)–(12) are a $(2N + 1)$-dimensional system. Its analysis is very complicated. Therefore, we use the mean-field approach. All terms in Eqs. (10)–(12) are averaged over the ensemble:

$$\langle \dot{x} \rangle = \langle f \rangle - \langle y \rangle - \langle c \rangle + q(z - \langle x \rangle), \tag{15}$$

$$\langle \dot{y} \rangle = \langle x \rangle - b\langle y \rangle, \tag{16}$$

$$\dot{z} = \omega_f(\langle x \rangle - z). \tag{17}$$

Here $\langle x \rangle$ is given by Eq. (14). Other mean values are defined in the same way:

$$\langle y \rangle = \frac{1}{N}\sum_{i=1}^{N} y_i, \quad \langle c \rangle = \frac{1}{N}\sum_{i=1}^{N} c_i, \quad \langle f \rangle = \frac{1}{N}\sum_{i=1}^{N} f(x_i). \tag{18}$$

Note that the coupling term $kN(\ldots)$ in Eq. (15) has conveniently disappeared, since $kN\langle \langle x \rangle - x_i \rangle = 0$. The only control term $q(z - \langle x \rangle)$ has been left. In addition, Eqs. (15)–(17) is a three-dimensional system. Though Eqs. (15)–(17) are not suitable to describe full dynamics of the mean field, because $\langle f \rangle \neq f(\langle x \rangle)$, they can be used to find the steady state of the mean field. If $ab < 1$ and for all i the $|c_i| \leqslant 1/b - a$, then $|x_{i0}| \leqslant 1$. According to the definition of $f(x_i)$, it is a linear function in the range $-1 \leqslant x_{i0} \leqslant 1$: $f(x_{i0}) = ax_{i0}$. Consequently, $\langle f \rangle_0 = a\langle x \rangle_0$. Eventually, the steady-state solution of

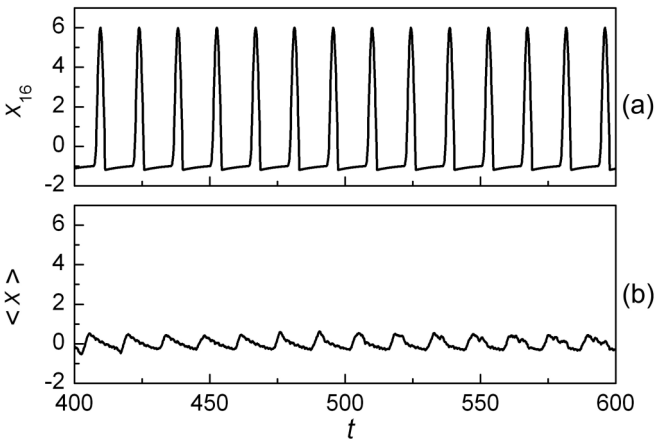

FIG. 4. Waveforms of isolated uncontrolled oscillators. $k = q = 0$. (a) Individual variable x_{16} and (b) mean variable $\langle x \rangle$.

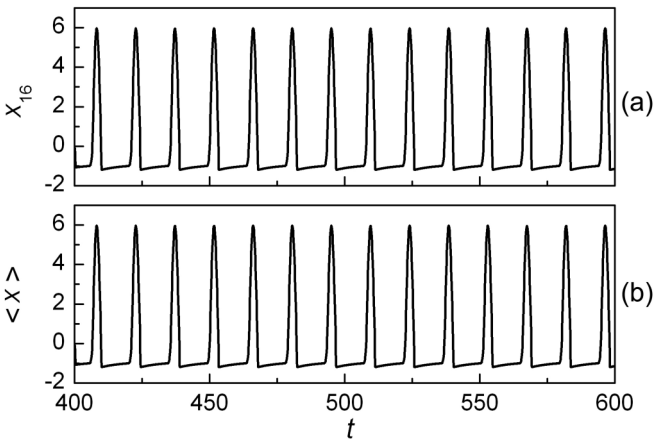

FIG. 5. Waveforms of coupled uncontrolled oscillators. $k = 0.3$, $q = 0$. (a) Individual variable x_{16} and (b) mean variable $\langle x \rangle$.

Eqs. (15)–(17) reads:

$$\langle x \rangle_0 = -\frac{b\langle c \rangle}{1 - ab}, \quad \langle y \rangle_0 = -\frac{\langle c \rangle}{1 - ab}, \quad z_0 = \langle x \rangle_0. \tag{19}$$

Now we linearize Eqs. (15)–(17) around the fixed point (19):

$$\langle \dot{x} \rangle = a\langle x \rangle - \langle y \rangle + q(z - \langle x \rangle), \tag{20}$$

$$\langle \dot{y} \rangle = \langle x \rangle - b\langle y \rangle, \tag{21}$$

$$\dot{z} = \omega_f(\langle x \rangle - z). \tag{22}$$

Note that Eqs. (20)–(22) do not include parameter $\langle c \rangle$. The characteristic equation has the following algebraic form:

$$\begin{aligned} &\lambda^3 + h_2\lambda^2 + h_1\lambda + h_0 = 0, \\ &h_2 = q - a + b + \omega_f, \\ &h_1 = bq + 1 - ab - (a - b)\omega_f, \\ &h_0 = (1 - ab)\omega_f. \end{aligned} \tag{23}$$

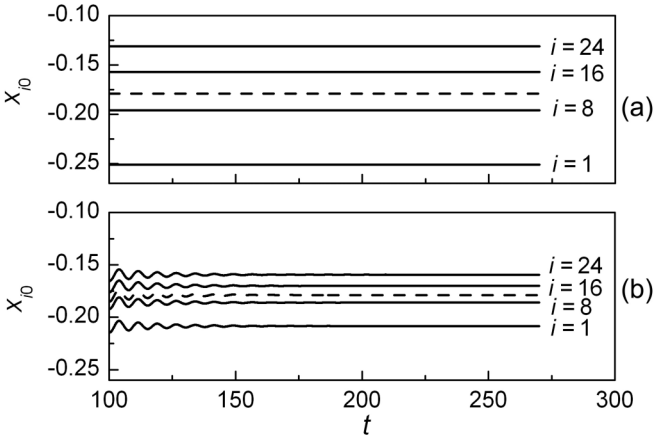

FIG. 6. Steady states. (a) Isolated uncontrolled oscillators, $k = q = 0$, from formula $x_{i0} = -bc_i/(1 - ab)$. The dashed line is $\langle x \rangle_0 = -0.18$ from formula (19). (b) Coupled controlled oscillators from Eqs. (10)–(12), $k = 0.3$, $q = 3$, $\omega_f = 0.1$. The dashed line is at -0.18.

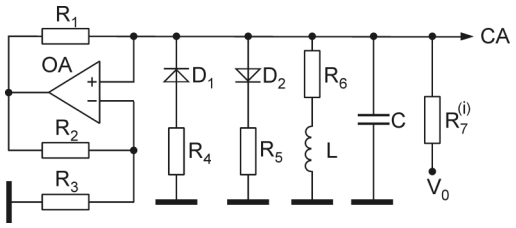

FIG. 7. Circuit diagram of a single FHN-type oscillator. CA is the coupling array [see Table I, outputs of all N individual oscillators are connected to the CA via "basement" (B)].

This cubic equation has been solved numerically for different values of the control parameter q. It has three eigenvalues $\lambda_1, \lambda_2, \lambda_3$. The maximal value of the real parts, $\max(\mathrm{Re}\lambda_{1,2,3})$, is plotted in Fig. 3. It becomes negative at $q \geqslant q_{\mathrm{th}} = 2.9$, indicating stability of the steady state (19).

Stability analysis of Eqs. (20)–(22) can be also performed analytically using the Hurwitz matrix:

$$H = \begin{bmatrix} h_2 & h_0 & 0 \\ 1 & h_1 & 0 \\ 0 & h_2 & h_0 \end{bmatrix}. \tag{24}$$

According to the Routh-Hurwitz stability criterion the system is stable if all diagonal minors of the H matrix are positive:

$$\Delta_1 = h_2 > 0, \quad \Delta_2 = h_2 h_1 - h_0 > 0,$$
$$\Delta_3 = h_2 h_1 h_0 - h_0^2 = h_0(h_2 h_1 - h_0) = h_0 \Delta_2 > 0. \tag{25}$$

Since $h_0 > 0$ it is sufficient to analyze Δ_1 and Δ_2. In the limit case of $\omega_f \to 0$ the $\Delta_2 \to h_2 h_1$. For $\omega_f \to 0$ the element $h_1 > 0$. Thus, the stability depends on the first minor $\Delta_1 = h_2$ only. The threshold control coefficient is found from a single inequality $h_2 > 0$: $q_{\mathrm{th}} = a - b$. In the case of finite ω_f both minors, Δ_1 and Δ_2, should be analyzed. For the specific parameter values $a = 3$ and $b = \omega_f = 0.1$, used further in the numerical simulations, we find from the inequalities (25) the threshold value of the control coefficient $q_{\mathrm{th}} = 2.9$ in excellent agreement with the plot in Fig. 3.

Numerical results obtained from Eqs. (10)–(12) for three different sets of the coupling-control parameters (1) [$k = q = 0$], (2) [$k \neq 0, q = 0$], and (3) [$k \neq 0, q \neq 0$] are presented in Figs. 4 to 6, respectively. The following dimensionless parameters have been used: $N = 24$, $a = 3$, $b = 0.1$, $c_i = 44/(24 + i)$, $d = 60$, $g = 3$.

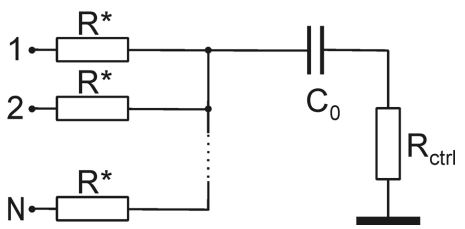

FIG. 8. Circuit diagram of the controller. $R^* C_0 R_{\mathrm{ctrl}}$ is a stable first-order branched filter. See formula (26) for definition of q and ω_f.

TABLE I. Map of connections in the coupling array CA.

8th floor										8-10
7th floor									7-9	7-10
6th floor								6-8	6-9	6-10
5th floor							5-7	5-8	5-9	5-10
4th floor						4-6	4-7	4-8	4-9	4-10
3rd floor					3-5	3-6	3-7	3-8	3-9	3-10
2nd floor				2-4	2-5	2-6	2-7	2-8	2-9	2-10
1st floor			1-3	1-4	1-5	1-6	1-7	1-8	1-9	1-10
G floor		1-2	2-3	3-4	4-5	5-6	6-7	7-8	8-9	9-10
B	1	2	3	4	5	6	7	8	9	10

IV. ELECTRONIC EXPERIMENT

Experiments have been carried out using an array of FHN-type oscillators, described in detail elsewhere [20]. A single oscillator is sketched in Fig. 7. The OA is an NE5534 operational amplifier, and the $D_{1,2}$ are general-purpose BAV99 type diodes ($V^* = 0.6$ V, the breakpoint voltage of the $I - V$ characteristic). The following values of the circuit elements have been set: $L = 10$ mH, $C = 3.3$ nF, $R_1 = R_2 = 1$ kΩ, $R_3 = 510$ Ω, $R_4 = 30$ Ω, $R_5 = 510$ Ω, $R_6 = 275$ Ω (resistor 220 Ω in series with coil resistance 55 Ω), $R_7^{(i)} = (24 + i)$ kΩ, $V_0 = -15$ V.

Figure 8 schematically illustrates the controller. The adjustable resistance R_{ctrl} can be set positive (to decrease the control coefficient, $q < \rho/R^*$), to zero (to ground the capacitor C_0 and to set $q = \rho/R^*$), or negative (to increase the control coefficient, $q > \rho/R^*$). In the latter case, a negative impedance converter should be employed.

The coupling array (CA) for the all-to-all configuration ($N = 10$) has been built using multi-story construction (Table I), starting from the "basement" (B) for connecting the oscillators, then rising to the ground floor (G), and eventually going to the 8th floor, used for coupling the cells. The number of coupling resistors is given by $M = N(N-1)/2$, e.g., for $N = 10$ the $M = 45$.

Dimensionless variables and parameters in Eqs. (10)–(13) are related to the circuit variables and element values in Fig. 7

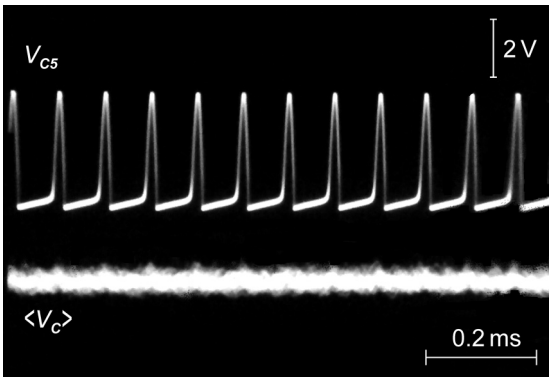

FIG. 9. Waveforms of isolated uncontrolled oscillators, individual variable V_{C5} and mean variable $\langle V_C \rangle$. $R_m \to \infty$.

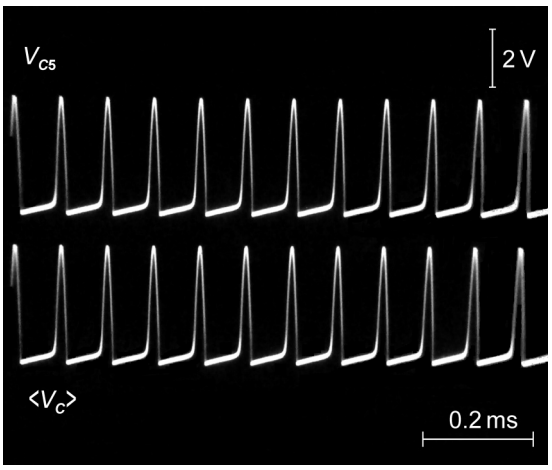

FIG. 10. Waveforms of coupled uncontrolled oscillators, individual variable V_{C5} and mean variable $\langle V_C\rangle$. $R_m = 5.6$ kΩ, $R^* \to \infty$.

and Fig. 8 as follows:

$$x_i = \frac{V_{Ci}}{V^*},\ y_i = \frac{\rho I_{Li}}{V^*},\ z = \frac{V_{C_0}}{V^*},\ t \to \frac{t}{\sqrt{LC}},\quad \rho = \sqrt{\frac{L}{C}},$$
$$a = \frac{\rho}{R_3},\quad b = \frac{R_6}{\rho},\quad c_i = \frac{\rho V_0}{R_7^{(i)} V^*},\quad d = \frac{\rho}{R_4},\ g = \frac{\rho}{R_5},$$
$$k = \frac{\rho}{R_m},\quad q = \frac{\rho}{R^* + NR_{\rm ctrl}},\quad \omega_f = \frac{N\sqrt{LC}}{(R^* + NR_{\rm ctrl})C_0}. \tag{26}$$

Here V_C is the voltage across the capacitor C and I_L is the current through the inductor L in Fig. 7. V_{C_0} is the voltage across the external control capacitor C_0, R_m is the mutual coupling resistance between two oscillators, R^* is the coupling resistance between the controller and an individual oscillator, and $R_{\rm ctrl}$ is the adjustable resistance of the controller in Fig. 8.

Typical experimental signals taken from the screen of a multichannel analog oscilloscope for $N = 10$ are presented in Figs. 9 and 10. They are in a good agreement with the corresponding numerical plots in Figs. 4 and 5, respectively.

Instead of experimental photos (several horizontal lines) demonstrating constant (stabilized) steady states, we present in Table II measured voltages V_{C0}. The employed digital dc voltmeter has higher accuracy than an analog oscilloscope. Note that the mean value $\langle V_{C0}\rangle = -298$ mV is the same for both, the array of isolated and the array of coupled controlled oscillators.

TABLE II. Stabilized steady states. Isolated damped oscillators, $R_m \to \infty$. Coupled controlled oscillators, $R_m = 5.6$ kΩ, $R^* = 240$ Ω, $R_{\rm ctrl} = 0$, $C_0 = 2.2$ μF. $N = 10$. $\langle V_{C0}\rangle$ is the mean of all N oscillators.

V_{C0}	Isolated damped osc.	Coupled controlled osc.
$V_{C0}^{\max}$ (mV)	−211	−279
$\langle V_{C0}\rangle$ (mV)	−298	−298
$V_{C0}^{\min}$ (mV)	−360	−314

The threshold coupling resistance $R^*_{\rm th}$ is about 560 Ω (stabilization can be achieved for $R^* < R^*_{\rm th}$). The corresponding dimensionless value, estimated using formula (26), is $q_{\rm th} \approx 3.1$ (for $\rho = 1.74$ kΩ and $R_{\rm ctrl} = 0$), which is in reasonable agreement with the numerical value $q_{\rm th} = 2.9$ in Fig. 3. The experimental results presented in Table II have been obtained for $R^* = 240$ Ω, which corresponds to the dimensionless value $q = 7.25$.

V. CONCLUDING REMARKS

The performed analytical, numerical, and experimental investigation of the all-to-all globally coupled FitzHugh-Nagumo–type oscillators with separate coupling and control networks and the stabilization of the steady states by means of the stable first-order RC branched filter induce the following conclusions.

All-to-all global coupling, in comparison with star global coupling, exhibits a significantly stronger interaction by a factor of N [see formula (8)], where N is the number of the involved oscillators. This result could be intuitively predicted.

An important advantage of a separate control network is the possibility to set the control parameter q above the threshold $q_{\rm th}$ independently of the intrinsic coupling parameter kN. The threshold $q_{\rm th}$ does not depend on the intrinsic bilateral coupling coefficient k. In Eq. (23) and in the Hurwitz matrix (24) the h parameters do not include coefficient k.

The dependence of the maximal value of the real parts of the eigenvalues $\lambda_{1,2,3}$ on q demonstrates that the steady states can be stabilized in a wide range of q above the $q_{\rm th}$. This is a convenient property of the controller in practical applications. Moreover, the control parameter $q = \rho/(R^* + NR_{\rm ctrl})$ [see formula (26)] can be easily tuned by the external controller via R^* (if accessible) and/or via $R_{\rm ctrl}$ (Fig. 8). The resistance of the controller $R_{\rm ctrl}$ can be set positive, to zero, or even negative. In the latter case a negative impedance converter should be employed to obtain $R_{\rm ctrl} < 0$.

An interesting result is that coupling of the oscillators does not change the mean value of the steady states. The $\langle x\rangle_0$ in Fig. 6 and $\langle V_{C0}\rangle$ in Table II are exactly the same in the array the isolated oscillators and in the array of coupled oscillators, whereas the individual steady states of the nonidentical oscillators depend on the coupling strength. They are less spread and are coming closer to the mean value in the coupled array (Fig. 6 and Table II) than in the isolated oscillators.

Concerning nonglobal connections, which may manifest in biological systems, the following remark should be added. To be specific, we consider the *nearest-neighbors coupling*, which is attributed to the class of local connection. In the case of the ring configuration, the coupling term reads: $Q = k(x_{i+1} - 2x_i + x_{i-1}),\ \ i = 1, \ldots, N,$ where $x_{N+1} \equiv x_1$ and $x_0 \equiv x_N$. Using the same mean-field approach as in the case of global coupling, we find that the coupling term Q vanishes, because $k\langle x_{i+1} - 2x_i + x_{i-1}\rangle = \langle x\rangle - 2\langle x\rangle + \langle x\rangle = 0$. Thus, we come to Eqs. (15)–(17) and eventually to Eqs. (20)–(22), yielding the same results of the stability analysis, i.e., the same dependence $\mathrm{Re}\lambda(q)$ and the same value of $q_{\rm th}$.

[1] A. Stefański, *Determining Thresholds of Complete Synchronization, and Application* (World Scientific, Singapore, 2009).
[2] C. Sarkar and S. Jalan, Chaos **28**, 102101 (2018).
[3] A. Tamaševičius, E. Tamaševičiūtė, and G. Mykolaitis, Appl. Phys. Lett. **101**, 223703 (2012).
[4] A. Pikovsky, M. Rosenblum, and J. Kurths, *Synchronization: A Universal Concept in Nonlinear Sciences* (Cambridge University Press, Cambridge, 2003).
[5] V. Tiberkevich, A. Slavin, E. Bankowski, and G. Gerhart, Appl. Phys. Lett. **95**, 262505 (2009).
[6] B. Liu, Y. Braiman, N. Nair, Y. Lu, Y. Guo, P. Colet, and M. Wardlaw, Opt. Commun. **324**, 301 (2014).
[7] M. G. Rosenblum and A. S. Pikovsky, Phys. Rev. Lett. **92**, 114102 (2004).
[8] M. Rosenblum, N. Tukhlina, A. Pikovsky, and L. Cimponeriu, Int. J. Bifurcat. Chaos **16**, 1989 (2006).
[9] L. S. Tsimring, N. F. Rulkov, M. L. Larsen, and M. Gabbay, Phys. Rev. Lett. **95**, 014101 (2005).
[10] A. Tamaševičius, G. Mykolaitis, E. Tamaševičiūtė, and S. Bumelienė, Nonlinear Dyn. **81**, 783 (2015).
[11] I. Ratas and K. Pyragas, Phys. Rev. E **90**, 032914 (2014).
[12] O. V. Popovych, C. Hauptmann, and P. A. Tass, Phys. Rev. Lett. **94**, 164102 (2005).
[13] N. Tukhlina, M. Rosenblum, A. Pikovsky, and J. Kurths, Phys. Rev. E **75**, 011918 (2007).
[14] K. Pyragas, O. V. Popovych, and P. A. Tass, Europhys. Lett. **80**, 40002 (2007).
[15] K. Pyragas, V. Novičenko, and P. A. Tass, Biol. Cyber. **107**, 669 (2013).
[16] K. Pyragas and P. A. Tass, Lith. J. Phys. **56**, 223 (2016).
[17] E. Adomaitienė, G. Mykolaitis, S. Bumelienė, and A. Tamaševičius, Nonlin. Anal. Model. Contr. **22**, 421 (2017).
[18] E. Adomaitienė, S. Bumelienė, G. Mykolaitis, and A. Tamaševičius, Complexity **2017**, 324879 (2017).
[19] A.-L. Benabid, S. Chabardes, J. Mitrofanis, and P. Pollak, Lancet Neurol. **8**, 67 (2009).
[20] E. Tamaševičiūtė, G. Mykolaitis, and A. Tamaševičius, Nonlin. Anal. Model. Contr. **17**, 118 (2012).